IET Generation, Transmission & Distribution

Research Article

IET Journals
The Institution of Engineering and Technology

Optimal power flow in multi-terminal HVDC networks with embedded high-power DC–DC converters for voltage matching and flexible DC transmission

ISSN 1751-8687
Received on 9th August 2019
Revised 30th April 2020
Accepted on 10th June 2020
E-First on 9th July 2020
doi: 10.1049/iet-gtd.2019.1238
www.ietdl.org

Sawsan Sayed[1] ✉, *Ahmed Massoud*[1]

[1]*Department of Electrical Engineering, Qatar University, Doha, Qatar*

✉ *E-mail: sa1108530@student.qu.edu.qa*

Abstract: High-power DC–DC converters are integrated into multi-terminal high-voltage DC (MTDC) networks, typically for voltage matching or flexible DC transmission. This study addresses droop-controlled radial and mesh MTDC networks with transmission loss minimisation considering the impact of integrating a high-power DC–DC converter. DC voltage droop control can achieve minimum power loss in radial MTDC transmission network by controlling the power-sharing among the receiving nodes inversely proportional to their transmission line resistances. Updating the droop characteristics by an optimisation algorithm guarantees optimal power flow (OPF) during renewable source power generation fluctuation. Meanwhile, the mesh network DC voltage references can be updated by the OPF for transmission loss minimisation. This study presents the impact of incorporating a high-power DC–DC converter at different system access lines of a radial MTDC network while targeting efficient power transfer and DC transmission loss minimisation. The effect of introducing a high-power DC–DC converter on the droop characteristic settings during steady-state operation in a radial MTDC network is investigated. Moreover, the impact of a high-power DC–DC converter in mesh MTDC network with OPF operation is explored. To validate the presented concepts, the CIGRE B4 MTDC network is used as a benchmark system with a metaheuristic optimisation technique.

Nomenclature

V	DC voltage
I	DC current
P	injected or received power
K	grid-side converter droop characteristic
R	DC transmission line resistance
G	DC transmission line conductance
D	high-power DC–DC converter gain
ρ	voltage deviation coefficient

Subscripts

wi	ith wind-side converter
gj	jth grid-side converter
wDi	ith WSCD
grj	jth GSCD
gL	no-load grid DC voltage
μ_i	ith voltage level
max	maximum variable limit

1 Introduction

High-voltage direct current (HVDC) transmission networks have developed from point-to-point configuration to multi-terminal HVDC (MTDC) configuration (i.e. commonly radial and mesh configurations) to enhance the transmission infrastructure with high reliability and flexibility [1]. Future visions for transmission network expansion incorporate MTDC interconnection with the existing power network such as the European Supergrid [2] and DESERTIC visions [3]. The technological development introduces some challenges to the MTDC networks with the absence of common DC grid code, as the interconnection of DC transmission lines with different DC voltage levels [4]. Therefore, high-power DC–DC converters may be required for integrating two HVDC networks of different voltage levels [5–7]. In MTDC networks, a non-isolated DC–DC converter may be used to integrate voltage source converter (VSC) terminals of the same configuration topology (e.g. monopole or bipole) to operate at the same DC voltage level [8]. While isolated DC–DC converter is used to interconnect different MTDC configuration topologies and/or different operating DC voltage levels [8]. The DC–DC converter in the MTDC network can be a single DC port or multi-port DC hub for multiple regional MTDC interconnection [9, 10]. For MTDC regional interconnection, the DC–DC converter facilitates the DC fault isolation between different DC network zones and allows power flow control, which makes it an important building block in the MTDC network [10, 11].

Power flow balance in the MTDC network is achieved commonly via DC voltage droop control [12]. The power flow balance is affected by the transmission line voltage drops, the location of power injection deficit/surplus, and the adjustment of the droop characteristics [12]. Several studies have presented the droop controller design considering steady-state [13, 14], and abnormal MTDC network operation conditions [15, 16]. In addition, some studies aimed for DC voltage droop control design to achieve minimum transmission power losses via distributed controllers [17, 18], and central controller [19, 20]. The ultimate objective of these studies is to enhance the transmission efficiency of the MTDC network and reduce any possible additional transmission losses. Radial MTDC network can maintain sub-optimal power flow with droop characteristics adjusted for minimum transmission losses in case of power injection fluctuation [17]. While optimal power flow (OPF) can be achieved for radial and mesh MTDC networks via optimisation approach with communication requirements among converters terminals with the central controller [19]. However, all these studies considered OPF for radial and mesh MTDC networks with power injection control at the VSCs terminals, mostly excluding the impact of integrating high-power DC–DC converters [21, 22].

Many studies have investigated the integration of high-power DC–DC converters in the MTDC network for voltage matching [22], power flow control [8, 22], and fault isolation [11]. While the studies on OPF in MTDC network with high-power DC–DC converters are limited. In [1], an optimisation model is presented to minimise the transmission losses for mesh MTDC network while considering the high-power DC–DC converter. However, the main

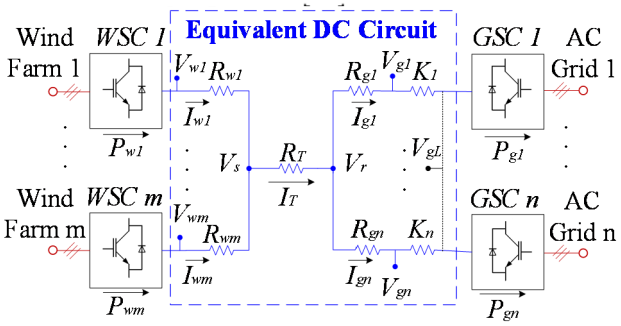

Fig. 1 *Radial MTDC network general configuration*

objective is to control the line power flow for a particular HVDC line while including the converter losses in the OPF algorithm. Nevertheless, neither the operation of the high-power DC–DC converter for network efficiency improvement nor the impact of introducing the high-power DC–DC converter on the power-sharing of the droop-controlled MTDC network has been considered. In [23], a high-power DC–DC converter is introduced to mesh MTDC network for power flow regulation while neglecting the DC–DC converter losses. The formulation of the MTDC network load flow through the secondary and primary control levels has been presented while considering the effect of line power flow control by the DC–DC converter. However, the OPF operation of the mesh network with transmission loss minimisation has not been considered.

The process of attaining the best possible usage of the available resources in a system can be achieved by an optimisation approach. That is through presenting the system's mathematical model, variables, constraints or satisfaction conditions, and properties, for best performance operation [24]. Several optimisation techniques have been developed that can be categorised into conventional methods and intelligent search methods [24, 25]. The conventional approaches are the Newton–Raphson optimisation, Lagrange multiplier method, and gradient method, which are considered as unconstrained optimisation approaches. Moreover, constrained optimisation methods can be divided into linear programming, non-linear programming, and quadratic programming. The conventional methods are suitable for many systems, yet they have limitations with the introduction of system uncertainties. Also, they are derivative-based optimisation approaches with single-path search area techniques, which raises the issue of possible local solutions [24, 25].

The intelligent search methods, or the metaheuristic optimisation techniques, have been developed to overcome complex problems that are susceptible to variables with uncertainties [24]. These techniques are based on the artificial replication process of the best natural features with natural selection and adaptation [24]. The metaheuristic algorithms are usually of non-deterministic and stochastic nature, thus realising an optimal solution. The two main classes of metaheuristic methods are the trajectory-based and population-based algorithms. The trajectory-based method is based on a single initial solution, and it commonly achieves a local optimum point. While the population-based method is based on a population of initial solutions with convergence tendency towards a global solution [24]. The popular evolutionary algorithms are the genetic algorithm (GA), particle swarm optimisation (PSO), and ant colony optimisation [26]. These techniques can vary in terms of the number of tuning parameters, computation time, and applied algorithm technique. However, the availability of some of these algorithms as commercial versions (e.g. GA in Matlab) with extensive programming background reduces the application complication [26]. The GA is based on natural biological evolution [27]. The main features of GA are code-based solution solver (i.e. not using solutions in their original forms), good exploration with population-based search, use of fitness function rather than derivatives, and search area based on probabilistic transition behavior [27]. The GA approach is popular due to its capabilities to handle several types of systems and constraints. Furthermore, due to its randomised-based search area, it is less likely to reach a local solution. The main demerit of the GA approach is the requirement of high computation time to converge to the optimal solution. Many studies have proved the GA's robustness and capability of attaining the optimal solution [28]. This paper employs the GA in the OPF controller layer of the MTDC network to attain flexible power transfer under efficient and stable operating conditions.

In this paper, OPF in MTDC networks with embedded high-power DC–DC converters for voltage matching and flexible DC transmission is investigated and assessed. A high-power DC–DC converter is introduced in droop-controlled radial and mesh MTDC networks. The impact is explored during normal network operation while considering OPF and droop characteristics design for minimum transmission losses. A high-power DC–DC converter is integrated into a radial MTDC network supported with a load flow model that is constrained to achieve efficient power transfer. Moreover, a high-power DC–DC converter is introduced in mesh MTDC network to control the power flow in the network with efficient power transfer according to the transmission system operator (TSO) requirements. CIGRE B4 network is used with a metaheuristic optimisation approach to present case studies. The contributions of this paper are summarised as follows.

- OPF in MTDC networks with embedded high-power DC–DC converters for voltage matching and flexible DC transmission.
- Investigating the impact of a high-power DC–DC converter integration on a droop-controlled radial MTDC network at different network access lines for flexible DC transmission (e.g. voltage enhancement) and interconnection of different high-voltage DC levels with minimum transmission losses during normal network operation.
- Investigating the impact of a high-power DC–DC converter in mesh MTDC network for efficient power transfer with OPF considering TSO requirements (i.e. for flexible DC transmission) during steady-state operation.

The structure of the rest of the paper is as follows. Section 2 presents the general concept of transmission loss minimisation and OPF in radial and mesh MTDC networks. Section 3 presents the incorporation of a high-power DC–DC converter in MTDC networks. Section 4 explores different scenarios of introducing a high-power DC–DC converter in a radial MTDC network at different access lines. Section 5 elucidates results for case studies of the presented concepts. Finally, Section 6 delivers the overall summary of the paper.

2 Optimal power flow in MTDC network

The power flow balance in the MTDC network is directly related to the regulation of the network DC voltage. The DC voltages of the network vary with the power injection fluctuation of renewable energy sources [29]. Several approaches with a combination of primary and secondary hierarchical control layers for MTDC networks have been presented in [17–20, 29]. The secondary control layer acquires the DC voltage setting required for the primary controller via an optimisation algorithm. The optimisation approach considers the MTDC network losses, including the transmission losses and converter losses, as an objective function for the OPF [30]. While the primary control layer, that is commonly a decentralised DC voltage droop controller, controls the renewable energy sources power-sharing at the receiving end nodes, such that multiple VSCs contribute to the network DC voltage control [30].

Considering wind farms as the available high-power renewable energy source, the general configuration of a radial MTDC network is shown in Fig. 1, for n grid-side converters (GSCs) and m wind-side converters (WSCs). The WSC is responsible for delivering the generated power from the wind farm to the MTDC network, while the GSC delivers the power received from the DC network to the AC grid. Therefore, during normal network operation, the WSCs operate in constant power control mode and deliver the total available power from the wind farms. While the GSCs operate in

Table 1 OPF equations for radial and mesh MTDC networks

	Equation	
general constraints	$0.95\ \text{pu} \le V_i \le 1.05\ \text{pu}$ for $i = 1, 2, \ldots, u$	(1)
	$-I_{L,\max,i} \le I_{L,i} \le I_{L,\max,i}$ for $i = 1, 2, \ldots, l$	
	$-P_{\max,i} \le P_i \le P_{\max,i}$ for $i = 1, 2, \ldots, (n+m)$	
	$-I_{\max,i} \le I_i \le I_{\max,i}$ for $i = 1, 2, \ldots, (n+m)$	
radial network	$P_{\text{DC,Lines}} = \sum_{i=1}^{m} G_{wi}(V_{wi} - V_s)^2$	(2)
	$+G_T(V_s - V_r)^2 + \sum_{j=1}^{n} G_{gj}(V_r - V_{gj})^2$	
	$I_{gj} = \dfrac{1/R_{gj}}{\sum_{j=1}^{n} 1/R_{gj}} I_T$	(3)
	$V_{gj} = I_T \dfrac{1}{\sum_{j=1}^{n} 1/R_{gj}}$	(4)
	$I_{wm} + \sum_{i=1}^{m-1} \dfrac{-V_s \pm \sqrt{V_s^2 + 4P_{wi}R_{wi}}}{2R_{wi}} - \sum_{j=1}^{n} I_{gj} = 0$	(5)
	$K_j = \dfrac{(V_{gj} - V_{gL})}{I_{gj}}$	(6)
	$V_{wi} - V_s - I_{wi}R_{wi} = 0$ for $i = 1, 2, \ldots, (m-1)$	(7)
mesh network	$P_{\text{DC,Lines}} = \sum_{i=1}^{m} \sum_{j=1}^{n} G_{ij}(V_i - V_j)^2$	(8)
	$a_u I_{\text{in},u} - b_u I_{\text{out},u} + \sum_{i=1}^{l_u} c_u I_{u,i} = 0$	(9)

where $I_{L,\max,i}$ and $I_{\max,i}$ are the current rating of the ith transmission line and VSC, respectively. G_T is the transmission line conductance for the line carrying the total current injected by the WSCs, I_T. I_{wm} is the DC current injected by the highest line drop WSC terminal. G_{ij} is the DC line conductance between the two node DC voltages V_i and V_j. a_u and b_u are constants with values 1 and 0, respectively, in case node u is a power controlled node, while 0 and 1, respectively, in case node u is a voltage controlled node. c_u is a constant with value 1 or −1 in case the current flow is into or out of node u, respectively. $I_{u,i}$ is the current flow to node u through the ith DC transmission line.

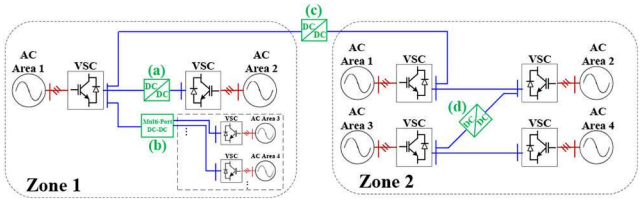

Fig. 2 *Multi-purpose high-power DC–DC converter integration into an MTDC network*

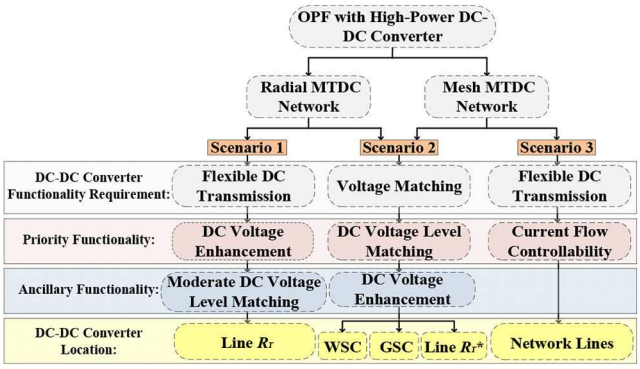

Fig. 3 *Functionality requirements of a high-power DC–DC converter in radial and mesh MTDC networks, where line R_T* is exclusive for the radial network*

DC voltage droop control mode [31]. The operating modes of the VSCs in an MTDC network are elaborated in [17, 31].

To accommodate the different VSC control modes according to the network requirements, a generalised voltage droop (GVD) control technique has been introduced in [32]. With the GVD method, the droop control, constant power control, and constant DC voltage control modes are achievable for a particular converter.

Minimum transmission loss in a radial MTDC network is attained if the power-sharing among the receiving nodes are controlled to be inversely proportional to their DC transmission lines resistances [17]. That is, while having the terminal with the highest line drop at the sending end operates at the maximum allowed DC voltage level (usually 5% of the nominal terminal voltage, which allows for a proper margin during transients [17]). Table 1 shows the optimisation objective function and constraints, for steady-state operation [18, 33, 34], required for the radial (i.e. considering Fig. 1) and mesh MTDC networks to minimise the DC lines losses, $P_{\text{DC,Lines}}$, with u DC node voltages and l DC transmission lines.

The GSCs' current injection and terminal DC voltage are shown in (3) and (4), respectively, for minimum transmission loss in the radial MTDC network shown in Fig. 1. Therefore, the GSCs droop characteristics, as shown in (6), are set according to (3) and (4). In the case of power injection fluctuation, the OPF controller updates the GSCs' droop characteristics. While the OPF controller updates the DC voltages references in case of a mesh network. The WSC that is assigned to a voltage of 1.05 pu for efficient power transfer is checked regularly during power injection variation to avoid over-voltage operation [33].

The optimisation functions shown in (2) and (8) are subjected to some constraints, boundaries, and non-linear non-equality constraints, as shown in (1), with respect to the network node DC voltages. These constraints take into consideration the transmission lines' current carrying capability, VSCs power rating, and the network load flow, as shown in (1), (5), and (7) for the radial network shown in Fig. 1. While the load flow for the mesh network depends on the network configuration with a general representation shown in (9).

Through the next section, OPF with minimum transmission loss in droop-controlled radial and mesh MTDC networks is presented considering high-power DC–DC converters.

3 High-power DC–DC converter in MTDC network for efficient power transfer

Several operational issues raise the prominence of high-power DC–DC converter integration into an MTDC, as multi-regional power-trading, system configuration matching, and line flow control, as shown in Fig. 2. The focus of this work is on the integration of a high-power DC–DC converter into a single-zone radial and mesh MTDC networks. Several approaches are studied, from the hierarchal control layers' point-of-view, to provide the best possible option for power transfer with power routing for loss minimisation. The study entails the load flow formulation and the optimum DC voltage control conditions and constraints for several configurations of a droop-controlled radial MTDC network, in addition to a mesh network, with a high-power DC–DC converter.

Incorporation of the high-power DC–DC converter at different access points of the MTDC network may improve the reliability and efficiency of the network. In this section, the high-power DC–DC converter is introduced in the MTDC network with several scenarios for flexible DC transmission and DC voltage matching. Fig. 3 shows the scenarios, which are further elaborated as follows.

- *Scenario 1: Flexible DC transmission in a radial MTDC network.* A major motivation for the development of MTDC networks is the experienced power transmission deficiency in AC transmission. In this scenario, the high-power DC–DC converter acts as a device that allows flexible DC transmission for efficiency improvement. For a radial MTDC network, as shown in Fig. 1, the voltage drop occurred due to the WSCs power injection may be mitigated by facilitating the power flow in the middle joint-line, R_T, through a high-power DC–DC converter. The high-power DC–DC converter output can be regulated to the highest allowed DC voltage operation, 1.05 pu, regardless of the WSCs power injection fluctuation. This enhances the power transmission efficiency of the radial

network. While to optimise further the DC power flow, the power distribution among the GSCs is required to be maintained inversely proportional to their DC transmission lines resistances according to (3) and (4), which is accomplished by the decentralised DC voltage droop controller.

- *Scenario 2: DC voltage matching in an MTDC network.* MTDC network is a modern and novel technology in power systems. Therefore, the absence of network infrastructure standards is inevitable. This leads to the possibility of confronting the interconnection between MTDC networks of different DC voltage levels. In the case of connecting additional WSCs and/or GSCs of different DC voltage levels to the existing radial network shown in Fig. 1, a high-power DC–DC converter is required corresponding to each WSC and/or GSC to match the MTDC voltage level. Moreover, in case of interconnection between WSCs and GSCs operating at two different DC voltage levels, a high-power DC–DC converter is required at the middle joint-line, R_T. In addition to DC voltage matching between the sending and receiving end nodes of the MTDC network, the high-power DC–DC converter can intrinsically boost the network efficiency by operating at the highest allowed DC output voltage level, 1.05 pu.
- *Scenario 3: Flexible DC transmission in a mesh MTDC network.* Meshed MTDC networks can have DC links with reverse power flow based on the geographical distribution of the WSCs and the electricity tariff at a certain time. To control the power flow in a particular DC line in meshed MTDC grids, an additional DC element is required in series to the DC line to control the current flow. A high-power DC–DC converter is introduced in this case for flexible DC transmission. This is further elaborated through a case study in Section 5. In case of WSCs and/or GSCs operating at different DC voltage levels than the mesh network voltage level, then the high-power DC–DC converter is required in a similar approach to the radial network (i.e. as elaborated in scenario 2).

The above categorisation is approached in this paper while tackling transmission losses minimisation in the DC grid by the decentralised DC voltage droop controller and the OPF controller.

Generally, the total power losses in an MTDC network is expressed in (10)

$$P_{\text{loss}} = \alpha P_{\text{DC,Lines}} + \beta P_{\text{DC-DC}} + \gamma P_{\text{VSC}} \tag{10}$$

where $P_{\text{DC,Lines}}$ is the DC transmission line's power losses. $P_{\text{DC-DC}}$ is the high-power DC–DC converters' power losses. P_{VSC} is the WSCs and GSCs' power losses.

This paper focuses on DC grid losses; therefore, WSCs and GSCs losses [20] are not considered (i.e. $\gamma = 0$ in (10)). The development of modular multi-level converter has led to several works that proposed highly-efficient high-power DC–DC converters [6, 7]. Nonetheless, the computation of the DC–DC converter non-negligible losses in high-power high-voltage applications is not straightforward. In [1], the losses of a DC–DC converter in mesh MTDC is considered quadratic to the average power transfer. However, this needs careful consideration for the development of new DC–DC converter technologies [1]. This paper takes into consideration the DC–DC converter losses similar to [20], considering a front-to-front high-power DC–DC converter (i.e. two VSC). The high-power DC–DC converter loss is computed by (11) and (12), considering a unity power factor, with the data provided in [20, 35, 36]

$$P_{\text{DC-DC}} = \sum_{i=1}^{s} 2 \times \left(P_c + V_c I_{\text{ac},i} + R_c I_{\text{ac},i}^2\right) \tag{11}$$

$$I_{\text{ac},i} = \frac{P_{\text{in},i}}{\sqrt{3}\, V_{\text{ac}}} \tag{12}$$

where P_c is the no-load losses in MW, V_c is the linearly dependent losses in Volt, and R_c represents the quadratically dependent losses in Ohm. $I_{\text{ac},i}$ is the current flow at the AC-side with operating AC voltage V_{ac} for the ith DC–DC converter. $P_{\text{in},i}$ is the input power to the ith DC–DC converter. s refers to the number of the DC–DC converter in the MTDC network.

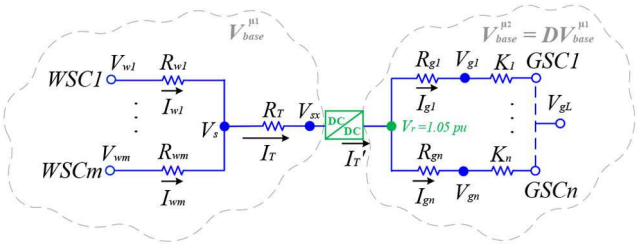

Fig. 4 *High-power DC–DC converter in radial MTDC network for flexible DC transmission, where $V_{base}^{\mu 1}$ and $V_{base}^{\mu 2}$ are the base voltages for the left and right-hand sides of the DC–DC converter, respectively*

The optimisation of the MTDC network has two sets of objectives in this work, which are transmission line losses and high-power DC–DC converters losses minimisation. The next section presents the radial network scenarios with the high-power DC–DC converter.

4 Scenarios for high-power DC–DC converter in radial MTDC network

The integration of a high-power DC–DC converter in a radial MTDC network is tackled in this section. Several scenarios are presented for an efficient and flexible DC power flow. The radial MTDC network consists of m WSCs that operate in constant power control mode, in addition to n GSCs that operate in DC voltage droop control mode. To maximise the transmission efficiency, the WSC with the highest line voltage drop terminal at node V_s, shown in Fig. 1, is assigned to 1.05 pu, as expressed in (13)

$$V_{wi}(\max\,(R_{wi} \cdot I_{wi})) = 1.05\ \text{pu} \tag{13}$$

where $i = 1, 2, \ldots, m$.

The high-power DC–DC converter in a DC grid acts similar to a transformer in AC systems with turns ratio that accommodates the different DC voltage levels across the DC network. Commonly for AC system studies, the AC network variables are put on a unified base and converted from the engineering unit to per-unit to eradicate the transformer effect [37, 38]. A similar approach is applicable for studies including DC–DC converter in MTDC networks in case of a non-unity gain converter. The per-unit base of the MTDC network lines resistances and current flow can be computed by (14) and (15) [38]

$$R_{\text{base}}^{\mu_i} = \frac{\left(V_{\text{base}}^{\mu_i}\right)^2}{P_{\text{base}}} \tag{14}$$

$$I_{\text{base}}^{\mu_i} = \frac{P_{\text{base}}}{V_{\text{base}}^{\mu_i}} \tag{15}$$

where $i = 1, 2, \ldots, p$ with p DC voltage level. $R_{\text{base}}^{\mu_i}$ (Ω), $V_{\text{base}}^{\mu_i}$ (kV), and $I_{\text{base}}^{\mu_i}$ (A) are the baseline resistance, base voltage, and base current, respectively, with reference to μ_i voltage level (i.e. as elaborated in Figs. 4–6).

4.1 Scenario 1: flexible DC transmission

To compensate for the voltage drop incurred in the radial MTDC network shown in Fig. 1, a high-power DC–DC converter can be considered at the joint-line (i.e. the line with resistance R_T), as shown in Fig. 4. The voltage drop at node V_{sx}, due to the WSCs transmission line resistances, is alleviated by controlling the high-power DC–DC converter gain for an output voltage as presented in (16). This results in efficient power transfer to the GSCs

$$V_r = 1.05\ \text{pu for } \forall 0.95\ \text{pu} \le V_{sx} < 1.05\ \text{pu} \tag{16}$$

where V_r and V_{sx} are with reference to $V_{\text{base}}^{\mu_1}$ and $V_{\text{base}}^{\mu_2}$, respectively.

In addition, to enrich the DC power transmission efficiency, the power-sharing among the GSCs can be adjusted for minimum power loss. The load flow for the radial network of Fig. 4 with transmission loss minimisation is derived, as presented in Table 2. To achieve transmission power loss minimisation in this case, the droop characteristics for the GSCs are designed as presented in (6) by using (21) and (22).

In case of introducing the high-power DC–DC converter at the line R_T for voltage matching between the WSCs and the GSCs, the same load flow is obtained, as shown in Table 2. However, the high-power DC–DC converter gain needs to be adjusted for matching the high-voltage DC levels while imposing the DC–DC converter output to 1.05 pu.

4.2 Scenario 2: DC voltage matching

In case it is required to integrate additional WSCs and/or GSCs to a radial MTDC network, it is crucial to match the DC voltage levels across the DC grid. This entails the connection of a high-power DC–DC converter for DC voltage matching. WSCs that are operating at a different DC voltage level from the radial MTDC network DC voltage are referred to as WSCDs, which act in constant power control mode, with a generalised configuration shown in Fig. 5. To maximise the DC power transmission efficiency from the WSCD to the DC grid, some operating preferences are taken into consideration for the network shown in Fig. 5. For DC voltage matching at the wind-side, the WSC DC terminal with the highest line drop at the common interconnection node, V_s, is assigned to 1.05 pu (i.e. based on $V_{\text{base}}^{\mu_1}$), as presented in (13). While all the WSCDs terminal DC voltages, V_{wDi}, are assigned to 1.05 pu (i.e. based on $V_{\text{base}}^{\mu_1+i}$) for efficient power transfer, as shown in (23)

$$V_{wDi} = V_{L,wDi}\left(1 + \frac{1}{\rho}\right) \tag{23}$$

where $V_{L,wDi}$ is the DC voltage level of the ith WSCD. ρ is considered for a 5% DC voltage deviation $\forall i$ (e.g. for WSCD1 with a DC voltage level of ±200 kV then V_{wD1} = 420 kV).

The high-power DC–DC converters gains, D_i for $i = 1, 2, \ldots, s$, are controlled to ensure matching the DC voltage level between the WSCDs and the radial network. That is while being imposed to the voltage drop at V_s introduced from the WSC with the highest line drop, as expressed in (24)

$$D_i = \frac{V_s}{V_{wxi}} \text{ for } \min(V_s) = V_{wi} - \max(I_{wi} \cdot R_{wi}) \tag{24}$$

where V_{wi} is shown in (13).

Moreover, similar to scenario 1, the DC voltage droop controllers of the GSCs in Fig. 5 are adjusted for power-sharing with the objective of transmission losses minimisation. The derived load flow for the radial MTDC network with DC voltage matching at the wind side, as shown in Fig. 5, with s WSCDs, is presented in Table 3. The droop characteristics of the GSCs in Fig. 5 are designed by (6) for minimum transmission power loss while using (3), (4), and (28).

The GSCs operating at a different DC voltage level from the radial DC grid are referred to as GSCDs, which operate in DC voltage droop control mode, with a generalised configuration shown in Fig. 6. The considered operating preferences for efficient power transfer of the network in Fig. 6 are as follows. In case of DC voltage matching at the grid-side, the WSC DC line with the highest voltage drop is assigned to 1.05 pu terminal DC voltage, as presented in (13). The gain of the high-power DC–DC converter placed cascaded to the GSCD is controlled for matching the DC voltage level of the GSCD to the radial MTDC network DC-link voltage while imposing the DC–DC converter output voltage, V_{gxj},

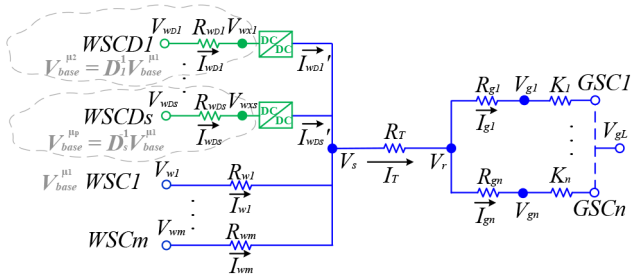

Fig. 5 *High-power DC–DC converters in radial MTDC network for voltage matching at the WSCs, where $V_{base}^{\mu_1}$ is the base voltage for the WSCs and GSCs while $V_{base}^{\mu_1+i}$ is the base voltage for the ith WSCD*

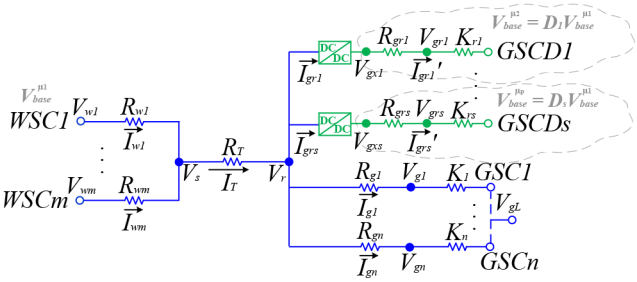

Fig. 6 *High-power DC–DC converters in radial MTDC network for voltage matching at the GSCs, where $V_{base}^{\mu_1}$ is the base voltage for the WSCs and GSCs while $V_{base}^{\mu_1+j}$ is the base voltage for the jth GSCD*

Table 2 Flexible DC transmission equations for radial network scenario 1 in Figs. 3 and 4

Converter	Equation	
WSC	$V_{wi} = \frac{V_r}{D} + I_{wi}R_{wi} + \sum_{i=1}^{m} I_{wi}R_T$	(17)
DC-DC Converter	$I_T{}' = \frac{1}{D}I_T = \frac{1}{D}\sum_{i=1}^{m} I_{wi}$ (lossless converter)	(18)
	$I_T{}' = \frac{(V_{sx}I_T) - P_{DC-DC}}{V_r}$ (converter with losses)	(19)
	$D = \frac{V_r}{V_{sx}}$	(20)
GSC	$I_{gj} = \frac{R_{th}}{R_{gj}} I_T{}' \text{ for } R_{th} = \frac{1}{\sum_{j=1}^{n} \frac{1}{R_{gj}}}$	(21)
	$V_{gj} = I_T{}' R_{th}$	(22)

Where the equations with green colour are relevant to the high-power DC–DC converter output-side load flow.

to 1.05 pu (i.e. based on $V_{\text{base}}^{\mu_1+j}$) for efficient power transfer, as shown in (32)

$$D_j = \frac{V_{gxj}}{V_r} \text{ for } V_{gxj} = V_{L,grj}\left(1 + \frac{1}{\rho}\right) \tag{32}$$

where $V_{L,grj}$ is the DC voltage level of the jth GSCD. ρ is considered for 5% DC voltage deviation operation $\forall j$.

Table 4 presents the derived load flow for the radial MTDC network, shown in Fig. 6, with DC voltage matching at the grid side with s GSCDs. In this case, the droop characteristics design for minimum transmission loss condition for the GSCs, K_j, are obtained by (6) using (37), (41), and (42). While the droop characteristics for the GSCDs, K_{rj}, are obtained by (6) using (35)–(40) for minimum power loss operation.

Table 3 Voltage matching equations at WSCs for radial network scenario 2 in Figs. 3 and 5

Converter	Equation	
WSC	$V_{wi} = V_{gL} + R_{wi}I_{wi} + \sum_{i=1}^{m} I_{wi}R_t + \sum_{i=1}^{s} I_{wDi}{}'R_t$	(25)
	$R_t = R_T + \frac{1}{\sum_{j=1}^{n}\frac{1}{R_{gj}+K_j}}$	(26)
WSCD	$V_{wDi} = \frac{V_{gL}}{D_i} + I_{wDi}{}'D_iR_{wDi} + \sum_{i=1}^{s} I_{wDi}{}'\frac{R_t}{D_i} + \sum_{i=1}^{m} I_{wi}\frac{R_t}{D_i}$	(27)
	$I_T = \sum_{i=1}^{m} I_{wi} + \sum_{i=1}^{s} I_{wDi}{}'$	(28)
DC-DC Converter	$D_i = \frac{V_s}{V_{wxi}}$	(29)
	$I_{wDi}{}' = \frac{1}{D_i}I_{wDi}$ (lossless converter)	(30)
	$I_{wDi}{}' = \frac{(V_{wxi}I_{wDi}) - P_{DC-DC}}{V_s}$ (converter with losses)	(31)

Where the green colour is related to the high-power DC–DC converter input-side load flow equations.

Table 4 Voltage matching equations at GSCs for radial network scenario 3 in Figs. 3 and 6

Converter	Equation	
WSC	$V_{wi} = V_{gL} + R_{wi}I_{wi} + \sum_{i=1}^{m} I_{wi}R_T + \sum_{i=1}^{m}\sum_{j=1}^{n} I_{wi}\frac{R_{th1}R_{th2}}{R_{gj}}$	(33)
	$R_{th1} = \frac{1}{\sum_{j=1}^{n}\frac{1}{R_{gj}+K_j}}$; $R_{th2} = \frac{1}{\sum_{j=1}^{n}\frac{1}{R_{gj}} + \sum_{j=1}^{s}\frac{1}{R_{grj}}}$	(34)
DC-DC Converter	$D_j = \frac{V_{gxj}}{V_r}$	(35)
	$I_{grj} = \frac{R_{th2}}{R_{grj}}I_T$	(36)
	$I_T = \sum_{i=1}^{m} I_{wi} = \sum_{j=1}^{s} I_{grj} + \sum_{j=1}^{n} I_{gj}$	(37)
	$I_{grj}{}' = \frac{1}{D_j}I_{grj}$ (lossless converter)	(38)
	$I_{grj}{}' = \frac{V_rI_{grj} - P_{DC-DC}}{V_{gxj}}$ (converter with losses)	(39)
GSCD	$V_{grj} = V_{gxj} - R_{grj}I_{grj}{}'$	(40)
GSC	$I_{gj} = \frac{R_{th2}}{R_{gj}}I_T$	(41)
	$V_{gj} = V_r - R_{gj}I_{gj}$	(42)

Where the high-power DC–DC converter output-side load flow is indicated by the green-coloured equations.

5 Results and discussion

5.1 Metaheuristic optimisation: genetic algorithm

GA optimisation relies on an iterative process for the survival of the best solutions, which will participate in the generation of the next population. This iterative operation is used to obtain an optimal-point for problems of the following formulation [39]:

$$\begin{aligned} &\min f(\boldsymbol{V}) \quad \text{s.t.} \\ &e(\boldsymbol{V}) = 0 \text{ and } n(\boldsymbol{V}) \le 0 \text{ for } \boldsymbol{V} \in S \end{aligned} \tag{43}$$

where f is the objective function (i.e. represented by (10)). e and n are the equality and non-equality constraint functions, respectively. S is the optimisation search area. $\boldsymbol{V}$ is the optimised vector variable, that is the network DC voltages, $[V_1, V_2, \ldots, V_u]^{\mathrm{T}}$.

The formulation procedure of network loss minimisation, with the GA application, is as follows [40].

(i) Present the optimisation variable, $\boldsymbol{V}$, as a code (i.e. as binary or floating-point string), as shown in (44)

$$\begin{aligned} x_1 &= [00100\ldots11101] \\ x_2 &= [10101\ldots10100] \\ &\vdots \\ x_u &= [10111\ldots10111] \end{aligned} \tag{44}$$

where x_i is referred to as the ith gene. The set $\{x_1, x_2, \ldots, x_u\}$ is referred to as a chromosome. The number of genes in this application is the number of the DC node voltages.

(ii) Based on the selected population size, N_{GA}, initialise the population, $\boldsymbol{P}_{\mathrm{GA}}$, as shown in (45), with random chromosomes, within the search area

$$\boldsymbol{P}_{\mathrm{GA}} = \begin{bmatrix} x_{1,1}, x_{2,1}, \ldots, x_{u,1} \\ x_{1,2}, x_{2,2}, \ldots, x_{u,2} \\ \vdots \\ x_{1,N_{\mathrm{GA}}}, x_{2,N_{\mathrm{GA}}}, \ldots, x_{u,N_{\mathrm{GA}}} \end{bmatrix} \tag{45}$$

where $x_{i,j}$ refers to the ith gene in the jth chromosome.

(iii) Compute the fitness of the chromosomes in $\boldsymbol{P}_{\mathrm{GA}}$. The GA formulation is based on a maximisation problem, thus, for function minimisation, the fitness function, $\boldsymbol{F}_{\mathrm{GA}}$, is evaluated, as shown in (46)

$$\boldsymbol{F}_{\mathrm{GA}} = \frac{1}{f(\boldsymbol{x})} \text{ or } \boldsymbol{F}_{\mathrm{GA}} = -f(\boldsymbol{x}) \tag{46}$$

(iv) Select the chromosomes that give minimal fitness values to be passed for the new generation.

(v) Perform the process of crossover and mutation on the individual genes, and replace the past population with the new generation.

(vi) Evaluate the feasibility of the solution with the imposed constraints.

(vii) Repeat steps (iii) to (vi) for each new population generation.

(viii) Return the solution when the stopping criteria are met.

Fig. 7 shows a flowchart for the overall GA optimisation procedure. The optimisation performance of GA is governed by a set of parameters such as the population size, the crossover rate, the mutation rate, and the stopping criteria, which can influence the solution accuracy and computation time [24, 27]. If the choice of the population size is underestimated, then it is possible to achieve a local optimal solution, due to improper population evolution. While high population size can raise the rate of convergence. However, it also escalates the run time. Commonly, the selection of the size relies on the experience with the GA fitness function [24]. The crossover operation is based on swapping a segment of bits in a chromosome to a corresponding segment in another chromosome, while the mutation operation is based on changing single bits randomly in a chromosome. For efficient GA evolution, the rate of crossover is preferred to be between 0.7 and 1, while the rate of mutation between 0.001 and 0.05 [41]. The GA produces different solutions at each program evaluation due to its stochastic nature. However, better results are obtained with a moderate increase in the number of generations [41].

In this paper, initially, N_{GA} is selected as 400. The number of generations is set as 200. The crossover rate is set to 0.8, while the mutation rate is based on the GA function, mutation-adapt-feasible, provided by the optimisation toolbox. The initialisation of the population is based on two vectors, $\boldsymbol{V}_g^{\mathrm{ini},1}$ and $\boldsymbol{V}_g^{\mathrm{ini},2}$, as elaborated later. The stopping criterion is based on the function tolerance, which is set to 1×10^{-10}, while the constraint tolerance is set to 1×10^{-13}. For the sake of results verification, the output of the GA approach will be compared to the *fmincon* toolbox, a non-linear program solver with a local function minimisation property, provided by the Matlab environment. The stopping criterion for the

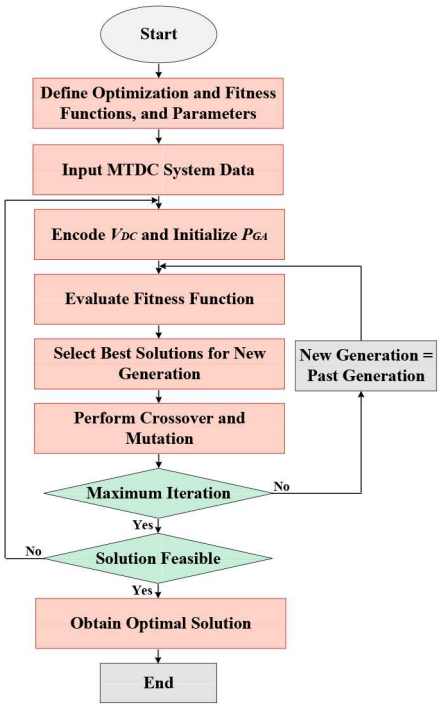

Fig. 7 *GA optimisation flowchart*

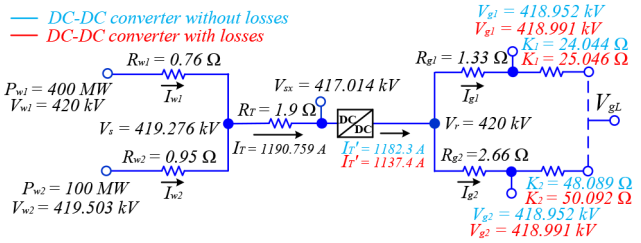

Fig. 8 *Case 1 results for a high-power DC–DC converter in the radial network, where* $V_{base}^{\mu 1} = 400\ kV$ *and* $V_{base}^{\mu 2} = 402.864\ kV$

Table 5 Monetary impact of including a high-power DC–DC converter in the radial MTDC network

parameter	$P_{\text{loss},A}$	$P_{\text{loss},B}$	$P_{\text{loss},C}$
power loss, MW	4.696	4.676	23.432
parameter	$E_{\text{loss},A} - E_{\text{loss},B}$		$E_{loss,A} - E_{loss,C}$
losses, MWh/year	175.2		−164,127
cost, $	6237.1		−5842,921.2

Where $P_{\text{loss},A}$, $P_{\text{loss},B}$ and $P_{\text{loss},C}$ are the transmission losses without the DC–DC converter, with a lossless DC–DC converter, and with DC–DC converter, including the converter losses, respectively. E is the annual energy losses. That is while considering 35.6 ($) electricity tariff/MWh [44].

fmincon is set similar to the GA approach, while its initial solution is set to $\boldsymbol{V}_g^{\text{ini},1}$.

Three cases are presented in this section for the integration of a high-power DC–DC converter in a radial MTDC network for flexible DC transmission and DC voltage matching with efficient power transfer operation. In addition, a case study is presented for a mesh MTDC network with the incorporation of a high-power DC–DC converter for flexible DC transmission with OPF operation according to the TSO requirement. The International Council on Large Electric Systems (CIGRE) has developed HVDC benchmark systems to provide a unified platform for the HVDC grids [42]. The radial and mesh CIGRE B4 models are used in this section with a modified version [42, 43]. The modified CIGRE B4 network lines data are available in [43] for a DC-link voltage of ±200 and ±400 kV.

The selected base values for the radial MTDC network are 800 MW and ±200 kV with reference to the DC voltage terminal V_{w1} for all the radial network cases. The VSCs' power rating in the radial network is 800 MW.

5.2 Radial network case 1: flexible DC transmission

The configuration shown in Fig. 4 is designed for minimum transmission loss while considering a 4-terminal radial MTDC network with ±200 kV DC-link voltage, as shown in Fig. 8. The total power injection by the WSCs, $\sum_{i=1}^{2} P_{wi}$, is 500 MW, while the first WSC is assigned to 1.05 pu. As presented in Fig. 8, the high-power DC–DC converter enhances the network voltage drop at V_{sx} from 417 to 420 kV at V_r. In case the 4-terminal radial MTDC network operates without the incorporation of the high-power DC–DC converter, then the GSCs terminal DC voltage is 416 kV with droop characteristics 20.1 and 40.2 Ω for GSC1 and GSC2, respectively. Thus, the DC voltage enhancement at the grid-side with the integration of a high-power DC–DC converter, in this case, is ∼3 kV.

The radial network total DC transmission power loss and the monetary impact of introducing the high-power converter are illustrated in Table 5. Introducing a lossless high-power DC–DC converter to the radial MTDC network reduces the total transmission power loss consumption. The losses are reduced by 175.2 MWh compared to the network operation without the DC–DC converter, as shown in Table 5. While in the case of considering the high-power DC–DC converter losses, the radial network losses increase significantly to 164,127 MWh compared to the network without the DC–DC converter, as presented in Table 5. It can be seen that the GSCs' terminal DC voltages are almost identical with the presence of a lossless high-power DC–DC converter or with the converter losses. Either by discarding the losses of the DC–DC converter or by considering a highly efficient DC–DC converter, the enhancement of the network power transmission efficiency is negligible or may add more losses to the system.

The genetic optimisation technique in [41] is applied to validate the results presented in Fig. 8 by using the Matlab optimisation toolbox. Due to the stochastic nature of the GA, the initial values adjustment for the solutions is found by the *fmincon* toolbox. The optimisation function required in this case, in addition to the constraints (1) and (5) is shown in (47). That is for $m = 2$, $n = 2$, and $s = 1$

$$P_{\text{loss}} = \sum_{i=1}^{m} G_{wi}(V_{wi} - V_s)^2 + G_T(V_s - V_{sx})^2 + \sum_{j=1}^{n} G_{gj}(V_r - V_{gj})^2 + P_{\text{DC-DC}} \tag{47}$$

Fig. 9 shows the best fitness function at each generation with ten iterations, or runs, for case 1, that is, while considering a lossless DC–DC converter. As expected, due to the stochastic nature of the GA, the number of generations and the optimal fitness function obtained at each iteration are not identical. Figs. 9*a* and *b* shows the results considering the initial optimisation variables, $\boldsymbol{V}_g^{\text{ini},1}$, fixed to the no-load DC voltage, $\boldsymbol{V}_g^{\text{ini},1} = [400\,\text{kV}\ 400\,\text{kV}]^{\text{T}}$. While Figs. 9*c* and *d* show the results considering adjusting the initial values to the *fmincon* output solution, $\boldsymbol{V}_g^{\text{ini},2} = [418.952\,\text{kV}\ 418.952\,\text{kV}]^{\text{T}}$. The adjustment of the initial population for the GA is a critical point to achieve a global solution with less computation time. It can be seen that the global solution is achieved with $\boldsymbol{V}_g^{\text{ini},2}$. The GSCs' terminal DC voltage, as shown in Fig. 9*d*, are equivalent at seventh iteration, which gives an indication for achieving the power-sharing among the GSCs, in the radial network, with minimal transmission losses. The optimal transmission losses are attained with $\boldsymbol{V}_g^{\text{ini},2}$ at iteration 7 as 4.676 MW, and the time computation required for one iteration is 997.66 s. The presented data computation is based on Matlab 2014a (i.e. with variables format set to float), by using a normal Personal Computer (PC) of 2.60 and 2.81 GHz Central Processing Unit

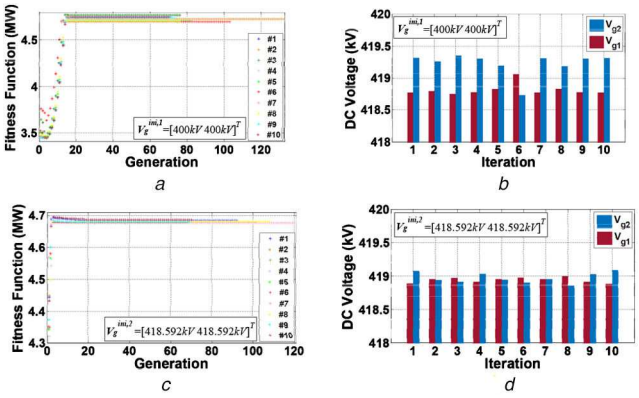

Fig. 9 *GA results for case 1 with lossless DC–DC converter*

(a), ***(c)*** Fitness function against the generations for $\boldsymbol{V}_g^{ini,1}$ and $\boldsymbol{V}_g^{ini,2}$, consecutively, ***(b)***, ***(d)*** The GSCs' terminal DC-voltage for ten iterations for $\boldsymbol{V}_g^{ini,1}$ and $\boldsymbol{V}_g^{ini,2}$, consecutively

Table 6 Impact of the GSCs' current rating uncertainty on the GA and *fmincon* methods based on $\boldsymbol{V}_g^{\text{ini},2}$

Approach		$I_{\max} = 500$ A
fmincon	P_{loss}	4.434 MW
	constraint	violation
	t_c	0.02 s
GA	P_{loss}	4.676 MW
	constraint	no-violation
	t_c	0.67 s

Where constraint refers to $I_T - I_{g1} - I_{g2} = 0$. t_c is the computation time taken by the employed approach.

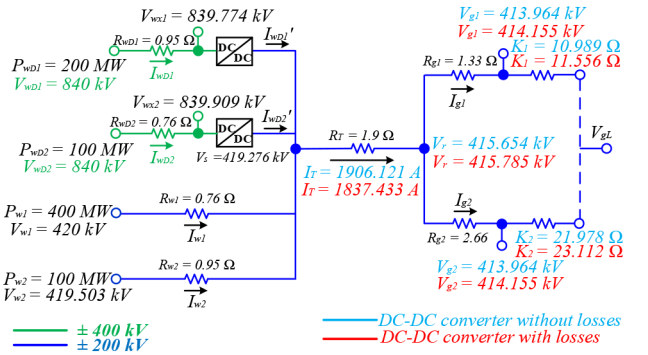

Fig. 10 *Case 2 results for high-power DC–DC converters in the radial network, where* $V_{base}^{\mu_1} = 400$ *kV,* $V_{base}^{\mu_2} = 801.165$ *kV, and* $V_{base}^{\mu_3} = 801.295$ *kV*

(CPU), with 12.0 GB RAM. However, it can be seen from Figs. 9*a* and *c* that the GA converges to its final solution around the 40th generation, with 100.8 s simulation time. For better GA performance with reduced execution time, less iterations, and enhanced convergence tendency, the population size and generation number can be set to 50 and 40, respectively. This adjustment results in obtaining the optimal solution within 19.88 s, meanwhile considering $\boldsymbol{V}_g^{\text{ini},2}$. The resultant time computation factor for the GA can be neglected in case of employing a vigorous computational framework, that is commonly available at the supervisory control level, with proper algorithm parameter tuning.

The obtained optimisation result from the GA method is verified with the *fmincon* approach. The power loss optimal solution obtained with the *fmincon* is 4.676 MW. Further studies and comparison of the Matlab optimisation techniques are available in [45, 46]. Nonetheless, compared to the GA, the performance of the *fmincon* can be affected by the system parameter uncertainty. Table 6 shows the impact of uncertainty on the GSCs' current rating capability, $I_{\max}$, on the performance of the GA and *fmincon* approaches. In this case, the actual current rating of the GSCs is 2000 A, but due to data-input error, the rating has been considered as 500 A. It can be seen from Table 6 that the *fmincon*, due to its non-stochastic nature, it produces an optimal power loss solution yet with power flow constraint violation. Whereas the GA approach can achieve the optimal solution while being restricted to the network power flow constraint.

5.3 Radial network case 2: DC voltage matching at the wind-side

For the case of DC voltage matching at the wind-side, a 4-terminal radial MTDC network is considered with a DC-link voltage of ±200 kV with a configuration similar to Fig. 1. In addition, two WSCDs are integrated into the radial network with a DC voltage level ±400 kV, as shown in Fig. 10. The 4-terminal radial MTDC network is expanded to 6-terminals with the interconnection of the WSCDs, as shown in Fig. 10. The total power injection from the WSCDs, $\sum_{i=1}^{2} P_{wDi}$, is 300 MW, while the total power injection from the WSCs, $\sum_{i=1}^{2} P_{wi}$, is 500 MW. The high-power DC–DC converters gains are controlled to match the DC voltage level between the radial MTDC network and the WSCDs DC voltage level. That is while imposing the DC–DC converter gain to the wind-side common interconnection node voltage, V_s, for efficient power transfer, as presented in (24). In this case, the total power injected by the WSCs and the WSCDs is received by two GSCs.

For results validation of Fig. 10, the objective function required for the implementation of the optimisation approach is shown in (48). That is for $m = 2$, $s = 2$, and $n = 2$, in addition to the constraints shown in (1) and (5)

$$P_{\text{loss}} = \sum_{i=1}^{m} G_{wi}(V_{wi} - V_s)^2 + \sum_{i=1}^{s} G_{wDi}(V_{wDi} - V_{wxi})^2 + G_T(V_s - V_r)^2 + \sum_{j=1}^{n} G_{gj}\left(V_r - V_{gj}\right)^2 + P_{\text{DC-DC}} \tag{48}$$

5.4 Radial network case 3: DC voltage matching at the grid-side

In this case, a 4-terminal radial MTDC network is considered with a configuration similar to Fig. 1 with a DC-link voltage ±200 kV. That is, while incorporating two additional VSCs at the grid-side of different DC voltage level than the radial network, that is with ±400 kV voltage level, as shown in Fig. 11. The 4-terminal radial network is expanded to a 6-terminal network while considering the GSCDs with ±400 kV voltage level, as shown in Fig. 11. The total power injection from the WSCs, $\sum_{i=1}^{2} P_{wi}$, is 500 MW. It can be seen from Fig. 11 that the GSCs terminal DC voltages are equal. While the GSCDs terminal DC voltages are equal in case of a lossless DC–DC converter. As the power distribution among the GSCs and GSCDs is based typically on their transmission line resistances to achieve transmission loss minimisation [17]. However, in case of considering the DC–DC converter losses, efficient power transfer is achieved but with non-equal GSCDs terminal DC voltages.

The optimisation objective function required in this case for results verification is shown in (49), in addition to the constraints shown in (1) and (5). That is for $m = 2$, $n = 2$, and $s = 2$

$$P_{\text{loss}} = \sum_{i=1}^{m} G_{wi}(V_{wi} - V_s)^2 + G_T(V_s - V_r)^2 + \sum_{j=1}^{n} G_{gj}\left(V_r - V_{gj}\right)^2 + \sum_{j=1}^{s} G_{grj}\left(V_{gxj} - V_{grj}\right)^2 + P_{\text{DC-DC}} \tag{49}$$

5.5 Mesh network case study: flexible DC transmission

In this case study, the impact of introducing a high-power DC–DC converter in mesh MTDC network is investigated from the

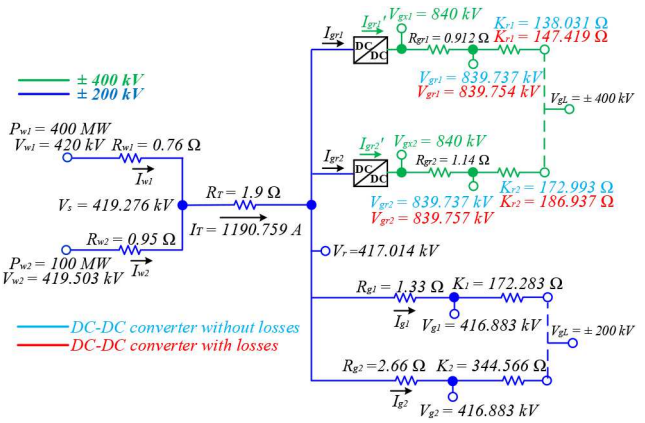

Fig. 11 *Case 3 results for high-power DC–DC converters in the radial network, where* $V_{base}^{\mu 1} = 400$ *kV,* $V_{base}^{\mu 2} = 805.728$ *kV, and* $V_{base}^{\mu 3} = 805.728$ *kV*

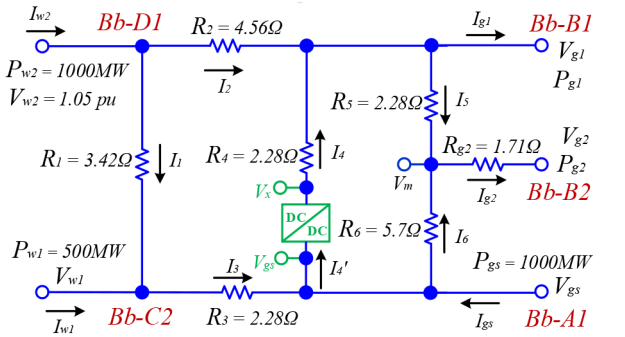

Fig. 12 *Modified CIGRE B4 mesh MTDC network DC equivalent circuit with high-power DC–DC converter at location 1, where Bb-C2 and Bb-D1 are the terminals of the first and second WSCs, respectively, Bb-A1 is the terminal of the VSC for the AC grid with voltage* V_{gs} *and power injection* P_{gs}*, and Bb-B1 and Bb-B2 are the terminals of the first and second GSCs, respectively*

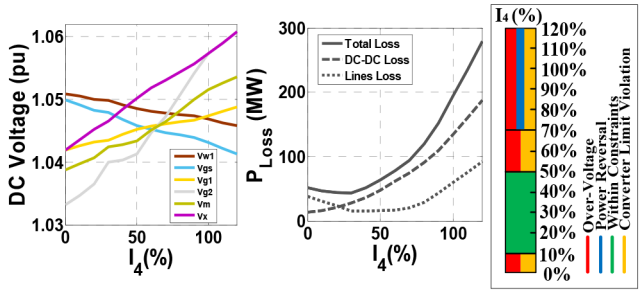

Fig. 13 *Results for a case study of a high-power DC–DC converter in modified CIGRE B4 mesh MTDC network with the DC voltages variations and power loss,* P_{Loss}*, with respect to the line current rating utilisation in location 1*

perspective of fulfilling the TSO requirement for flexible DC transmission. The main objective considered here is to control the current flow in a particular meshed DC line interconnection while achieving OPF operation. The modified CIGRE B4 mesh network shown in Fig. 12 is used in this study with a total power injection, $P_{gs} + \sum_{i=1}^{2} P_{wi}$, of 2500 MW to the mesh DC grid and a DC-link voltage ±400 kV. The VSCs ratings are 800, 1600, 2400, 1500, and 1700 MW for WSC1, WSC2, AC grid VSC, GSC1, and GSC2, respectively. While the transmission lines' current rating is 3500 A. In this study, the high-power DC–DC converter is introduced to the modified CIGRE B4 mesh network at three DC line locations. Location 1 is presented in Fig. 12.

The high-power DC–DC converter is cascaded to the meshed lines, in particular, to the lines that do not disturb the DC power flow in case of their outage. The current flow through the lines in these locations is controlled for 0–120% of the line current rating. The transmission lines can operate above their current rating for a specific duration of time. The optimisation approach applied in this study is constrained to (1) with the objective function presented in (8), in addition to the load flow equations of Fig. 12. The WSC2 DC terminal is assigned to 1.05 pu to avoid over-voltage operation during the global OPF operation for minimum power loss. The behaviour of the mesh network nodes DC voltage and the network power losses (i.e. considering both the lines losses and the DC–DC converter losses) with respect to the lines' current rating utilisation are presented in Fig. 13 for location 1. Similar results of locations 2 and 3 are presented in Fig. 14 while considering the transmission line losses only.

The graphical bar illustration in Figs. 13 and 14 is further elucidated by (50)

$$\zeta = \frac{I_x}{I_{\text{rating}}} 100\% \tag{50}$$

where I_x is the current flow at locations 1, 2, or 3 (i.e. I_4, I'_6, and I'_5, respectively), as shown in Figs. 12–14. I_{rating} is the DC line current rating. ζ is the utilisation factor of the DC line current rating.

Based on ζ of location 1, the mesh network in Fig. 12 has four operating regions, as presented in (51)

$$\zeta = \begin{cases} 0\% \le \zeta \le 10\% \text{ and} \\ 50\% \le \zeta \le 120\% \rightarrow \text{Over} - \text{Voltage} \\ 10\% < \zeta < 50\% \rightarrow \text{Within Constraints} \\ 70\% \le \zeta \le 120\% \rightarrow \text{Power Reversal} \\ 50\% \le \zeta \le 120\% \rightarrow \text{Converter Over Limit} \end{cases} \tag{51}$$

According to Fig. 13 and (51), it can be seen that for a line current rating utilisation between 10 and 50%, the network DC voltages and converters power flow are within the constraints. Otherwise, the network operates in over-voltage condition while violating the GSCs' power rating. In addition, with a line rating utilisation of 70% and above, one of the GSCs reverses the power direction, thus injecting power to the mesh network instead of supplying the power to the grid-side. Fig. 13 depicts the mesh network total power losses in addition to the transmission lines losses and the high-power DC–DC converter losses separately (i.e. the total power loss is the summation of these two losses). According to the selected line current operating range, it is possible to operate the mesh DC grid at a local minimum loss with respect to either the total losses, the DC–DC converter losses, or the DC lines losses. The high-power DC–DC converter losses are the main contributor to the mesh network losses, as depicted in Fig. 13. Nonetheless, with the technological development of the high-power DC–DC converter with reduced losses, the total power loss in the future may depend mainly on the transmission lines' losses. Similarly, the mesh network operating regions for location 2 and location 3 are obtained, as shown in Fig. 14. This shows the importance of infrastructure protection requirement against constraint violation in case of flexible DC transmission in a particular meshed DC grid line.

6 Conclusion

This paper presents DC voltage matching and flexible DC transmission scenarios of high-power DC–DC converter incorporation in droop-controlled radial MTDC network with droop characteristics adjusted for minimum transmission loss during normal network operation. In addition, this paper investigates the impact of a high-power DC–DC converter in mesh MTDC network with OPF for efficient power transfer and flexible DC transmission. The high-power DC–DC converter is introduced to the radial network for matching the different DC voltage levels and for DC voltage enhancement. Furthermore, the high-power DC–DC converter is introduced to the interconnection of the lines of a mesh network to study the impact of OPF operation with the

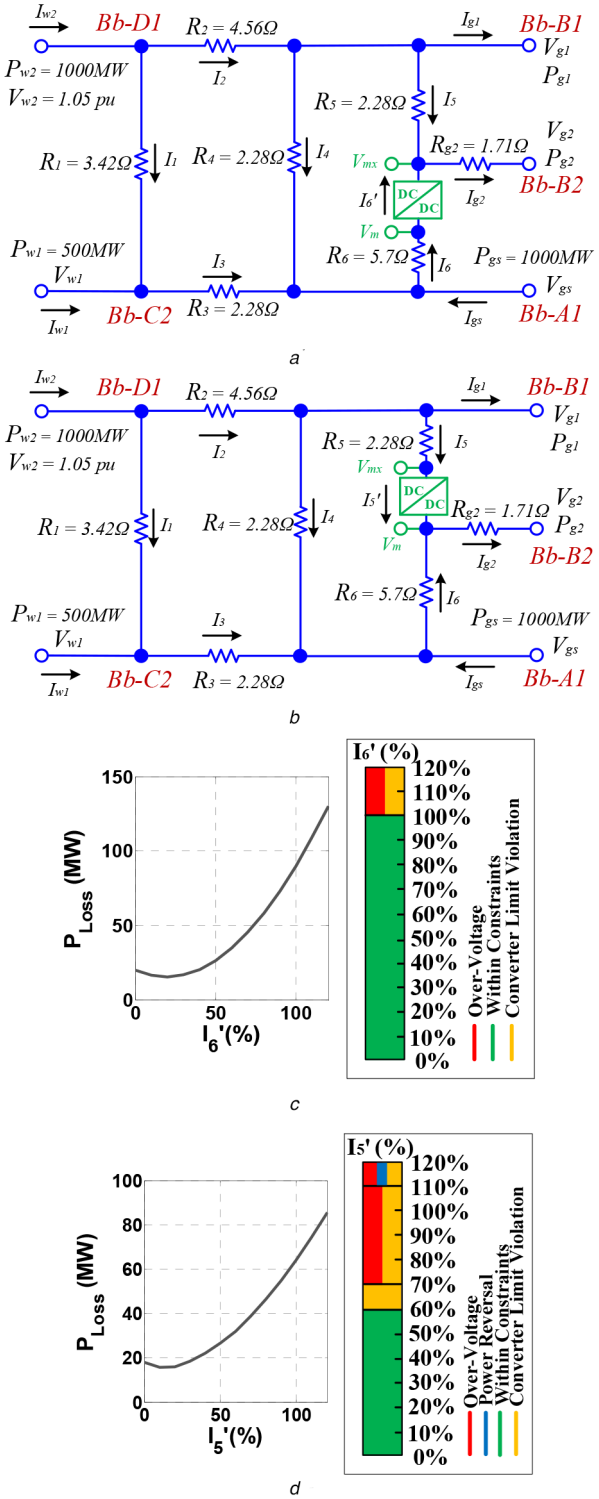

Fig. 14 *Modified CIGRE B4 mesh MTDC network with a case study of a high-power DC–DC converter in*
(a)–(c) Location 2, ***(b)–(d)*** Location 3

DC lines' current flow controllability according to the TSO requirements. CIGRE B4 system is used to deliver case studies for the scenarios.

7 Acknowledgments

This publication was made possible by NPRP grant NPRP (9-092-2-045) from the Qatar National Research Fund (a member of Qatar Foundation). The statements made herein are solely the responsibility of the authors.

8 References

[1] Garces, A., Montoya, D., Torres, R.: 'Optimal power flow in multiterminal HVDC systems considering DC/DC converters'. 2016 IEEE 25th Int. Symp. on Industrial Electronics (ISIE), Santa Clara, CA, 2016, pp. 1212–1217

[2] Pierri, E., Binder, O., Hemdan, N.G., *et al.*: 'Challenges and opportunities for a European HVDC grid', *Renew. Sust. Energy Rev.*, 2017, **70**, pp. 427–456

[3] Taggart, S., James, G., Dong, Z., *et al.*: 'The future of renewables linked by a transnational Asian grid', *Proc. IEEE*, 2012, **100**, (2), pp. 348–359

[4] Lüth, T., Merlin, M.M.C., Green, T.C., *et al.*: 'High-frequency operation of a DC/AC/DC system for HVDC applications', *IEEE Trans. Power Electron.*, 2014, **29**, (8), pp. 4107–4115

[5] Denniston, N., Massoud, A.M., Ahmed, S., *et al.*: 'Multiple-module high-gain high-voltage DC-DC transformers for offshore wind energy systems', *IEEE Trans. Ind. Electron.*, 2011, **58**, (5), pp. 1877–1886

[6] Gowaid, I.A., Adam, G.P., Massoud, A.M., *et al.*: 'Quasi two-level operation of modular multilevel converter for use in a high-power DC transformer with DC fault isolation capability', *IEEE Trans. Power Electron.*, 2015, **30**, (1), pp. 108–123

[7] Gowaid, I.A., Adam, G.P., Massoud, A.M., *et al.*: 'Hybrid and modular multilevel converter designs for isolated HVDC–DC converters', *IEEE J. Emerging Sel. Topics Power Electron.*, 2018, **6**, (1), pp. 188–202

[8] Kolparambath, S.K., Suul, J.A., Tedeschi, E.: 'Analysis of DC/DC converters in multiterminal HVDC systems for large offshore wind farms'. 2015 Int. Conf. on Technological Advancements in Power and Energy (TAP Energy), Kollam, 2015, pp. 415–420

[9] Jovcic, D., Lin, W.: 'Multiport high-power LCL DC hub for use in DC transmission grids', *IEEE Trans. Power Deliv.*, 2014, **29**, (2), pp. 760–768

[10] Jovcic, D., Taherbaneh, M., Taisne, J., *et al.*: 'Developing regional, radial DC grids and their interconnection into large DC grids'. 2014 IEEE PES General Meeting | Conf. & Exposition, National Harbor, MD, 2014, pp. 1–5

[11] Rahman, M.H., Xu, L., Yao, L.: 'Protection of large partitioned MTDC networks using DC-DC converters and circuit breakers', *Protect. Control Modern Power Syst.*, 2016, **1**, (19), pp. 1–9, DOI link: https://doi.org/10.1186/s41601-016-0030-0

[12] Haileselassie, T.M., Uhlen, K.: 'Impact of DC line voltage drops on power flow of MTDC using droop control', *IEEE Trans. Power Syst.*, 2012, **27**, (3), pp. 1441–1449

[13] Liang, J., Jing, T., Gomis-Bellmunt, O., *et al.*: 'Operation and control of multiterminal HVDC transmission for offshore wind farms', *IEEE Trans. Power Deliv.*, 2011, **26**, (4), pp. 2596–2604

[14] Raza, A., Liu, Y., Rouzbehi, K., *et al.*: 'Power dispatch and voltage control in multiterminal HVDC systems: a flexible approach', *IEEE Access*, 2017, **5**, pp. 24608–24616

[15] Beerten, J., Eriksson, R., Belmans, R.: 'Influence of DC voltage droop settings on AC system stability'. 10th IET Int. Conf. on AC and DC Power Transmission (ACDC 2012), Birmingham, 2012, pp. 1–5

[16] Chaudhuri, N.R., Chaudhuri, B.: 'Adaptive droop control for effective power sharing in multi-terminal DC (MTDC) grids', *IEEE Trans. Power Syst.*, 2013, **28**, (1), pp. 21–29

[17] Abdel-Khalik, A.S., Massoud, A.M., Elserougi, A.A., *et al.*: 'Optimum power transmission-based droop control design for multi-terminal HVDC of offshore wind farms', *IEEE Trans. Power Syst.*, 2013, **28**, (3), pp. 3401–3409

[18] Khazaei, J., Miao, Z., Piyasinghe, L., *et al.*: 'Minimizing DC system loss in multi-terminal HVDC systems through adaptive droop control', *Electr. Power Syst. Res.*, 2015, **126**, pp. 78–86

[19] Aragüés-Peñalba, M., Egea-Àlvarez, A., Gomis-Bellmunt, O., *et al.*: 'Optimum voltage control for loss minimization in HVDC multi-terminal transmission systems for large offshore wind farms', *Electr. Power Syst. Res.*, 2012, **89**, pp. 54–63

[20] Aragüés-Peñalba, M., Egea-Àlvarez, A., Arellano, S., *et al.*: 'Droop control for loss minimization in HVDC multi-terminal transmission systems for large offshore wind farms', *Electr. Power Syst. Res.*, 2014, **112**, pp. 48–55

[21] Jovcic, D., Zhang, L.: 'LCL DC/DC converter for DC grids', *IEEE Trans. Power Deliv.*, 2013, **28**, (4), pp. 2071–2079

[22] Jovcic, D., Ooi, B.T.: 'Developing DC transmission networks using DC transformers', *IEEE Trans. Power Deliv.*, 2010, **25**, (4), pp. 2535–2543

[23] Rouzbehi, K., Candela, J.I., Luna, A., *et al.*: 'Flexible control of power flow in multiterminal DC grids using DC-DC converter', *IEEE J. Emerging Sel. Topics Power Electron.*, 2016, **4**, (3), pp. 1135–1144

[24] De León-Aldaco, S.E., Calleja, H., Aguayo Alquicira, J.: 'Metaheuristic optimization methods applied to power converters: a review', *IEEE Trans. Power Electron.*, 2015, **30**, (12), pp. 6791–6803

[25] Zhu, J.: '*Optimization of power system operation*' (IEEE Press, Piscataway (N.J.), 2015)

[26] AlRashidi, M.R., El-Hawary, M. E.: 'Survey of particle swarm optimization applications in electric power systems', *IEEE Trans. Evol. Comput.*, 2009, **13**, (4), pp. 913–918

[27] Ozdemir, A., Lim, J.Y., Singh, C.: 'Post-outage reactive power flow calculations by genetic algorithms: constrained optimization approach', *IEEE Trans. Power Syst.*, 2005, **20**, (3), pp. 1266–1272

[28] Farhat, I., El-Hawary, M.: 'Optimization methods applied for solving the short-term hydrothermal coordination problem', *Electr. Power Syst. Res.*, 2009, **79**, (9), pp. 1308–1320

[29] Gavriluta, C., Candela, I., Luna, A., *et al.*: 'Hierarchical control of HV-MTDC systems with droop-based primary and OPF-based secondary', *IEEE Trans. Smart Grid*, 2015, **6**, (3), pp. 1502–1510

[30] Li, X., Guo, L., Hong, C., *et al.*: 'Hierarchical control of multiterminal DC grids for large-scale renewable energy integration', *IEEE Trans. Sustain. Energy*, 2018, **9**, (3), pp. 1448–1457

[31] Gomis-Bellmunt, O., Liang, J., Ekanayake, J., *et al.*: 'Voltage-current characteristics of multiterminal HVDC-VSC for offshore wind farms', *Electr. Power Syst. Res.*, 2011, **81**, (2), pp. 440–450
[32] Rouzbehi, K., Miranian, A., Candela, J.I., *et al.*: 'A generalized voltage droop strategy for control of multiterminal DC grids', *IEEE Trans. Ind. Appl.*, 2015, **51**, (1), pp. 607–618
[33] Sayed, S., Massoud, A.: 'Minimum transmission power loss in multi-terminal HVDC systems: a general methodology for radial and mesh networks', *Alexandria Eng. J.*, 2019, **58**, (1), pp. 115–125
[34] Bianchi, F.D., Gomis-Bellmunt, O.: 'Droop control design for multi-terminal VSC-HVDC grids based on LMI optimization'. 2011 50th IEEE Conf. on Decision and Control and European Control Conf., Orlando, FL, 2011, pp. 4823–4828
[35] Beerten, J., Cole, S., Belmans, R.: 'A sequential AC/DC power flow algorithm for networks containing multi-terminal VSC HVDC systems'. IEEE PES General Meeting, Providence, RI, 2010, pp. 1–7
[36] Daelemans, G., Srivastava, K., Reza, M., *et al.*: 'Minimization of steady-state losses in meshed networks using VSC HVDC'. 2009 IEEE Power & Energy Society General Meeting, Calgary, AB, 2009, pp. 1–5
[37] Enns, M.K.: 'Object-oriented sequence-domain representation of transformers for network analysis', *IEEE Trans. Power Syst.*, 2001, **16**, (2), pp. 188–193
[38] Cooper, C.B.: 'IEEE recommended practice for electric power distribution for industrial plants', *Electron. Power*, 1987, **33**, (10), p. 658
[39] Stacchini de Souza, J.C., Do Coutto Filho, M.B., Roberto, M.L.R.: 'A genetic-based methodology for evaluating requested outages of power network elements', *IEEE Trans. Power Syst.*, 2011, **26**, (4), pp. 2442–2449
[40] Ozpineci, B., Tolbert, L.M., Chiasson, J.N.: 'Harmonic optimization of multilevel converters using genetic algorithms', *IEEE Power Electron. Lett.*, 2005, **3**, (3), pp. 92–95
[41] Yang, X.-S.: '*Engineering optimization: an introduction with metaheuristic applications*' (J. Wiley, Hoboken (N.J.), 2010)
[42] An, T., Zhou, X., Han, C., *et al.*: 'A DC grid benchmark model for studies of interconnection of power systems', *CSEE J. Power Energy Syst.*, 2015, **1**, (4), pp. 101–109
[43] Vrana, T.K., Yang, Y., Jovcic, D., *et al.*: 'The CIGRE B4 DC grid test system'. Available at https://www.researchgate.net/publication/265123030_The_Cigre_B4_DC_grid_test_system, accessed 27 December 2018
[44] 'Qatar general electricity & water corporation'. Available at https://www.km.com.qa/CustomerService/Pages/Tariff.aspx, accessed 31 July 2019
[45] IET: 'Parallel optimization in Matlab'. Department of Information Technology at Uppsala University, 2013, pp. 1–47
[46] IET: 'Parallel global optimization of ABB's metal process models using Matlab'. Department of Information Technology at Uppsala University, 2014, pp. 1–30